

# Electron density and carriers of the diffuse interstellar bands

P. Gnaciński<sup>1</sup>, J.K. Sikorski<sup>2</sup>, G.A. Galazutdinov<sup>3</sup>

<sup>1</sup> Institute of Theoretical Physics and Astrophysics, University of Gdańsk, ul. Wita Stwosza 57, 80-952 Gdańsk, Poland  
e-mail: pg@iftia.univ.gda.pl

<sup>2</sup> Institute of Experimental Physics, University of Gdańsk, ul. Wita Stwosza 57, 80-952 Gdańsk, Poland  
e-mail: fizjks@iftia.univ.gda.pl

<sup>3</sup> Korea Astronomy and Space Science Institute, 61-1 Whaam-dong, Yuseong-gu, Daejeon, 305-348, Republic of Korea  
e-mail: gala@boao.re.kr

## Abstract.

We have used the ionisation equilibrium equation to derive the electron density in interstellar clouds in the direction to 13 stars. A linear relation was found, that allows the determination of the electron density from the Mg I and Mg II column densities in interstellar medium. The comparison of normalised equivalent width of 12 DIBs with the electron density shows that the DIBs equivalent width do not change with varying electron density. Therefore the DIBs carriers (1) can be observed only in one ionisation stage, or (2) the DIBs are arising in cloud regions (cores or cloud coronas) for which we can not determine the electron density.

**Key words.** ISM: clouds — ISM: molecules — ionisation balance

## 1. Introduction

The Diffuse Interstellar Bands (DIBs) are broad absorption features, seen in the interstellar clouds. There are almost 300 DIBs known in the optical and NIR spectrum (Galazutdinov *et al.* (2000)). Despite of over 80 years of investigations their nature is still unknown (for a review, see Herbig (1995)). Many carriers have been proposed as the carriers of DIBs, e.g. solid particles, simple molecules, negative atomic ions, carbon chains, fullerenes.

In 1985 van der Zwet & Allamandola proposed polycyclic aromatic hydrocarbons (PAHs) as the source of DIBs. Since then it is a popular hypothesis. There are however problems with obtaining gas phase laboratory spectra of dehydrogenated and/or ionised PAHs to verify this hypothesis. Recently Cox & Spaans (2006) have presented simulations of PAH charge state distribution in various environments. In clouds with various irradiation and density the fractional abundances of PAH cations, neutrals and anions changes dramatically.

We have used the ionisation equilibrium equation to obtain the electron densities in individual clouds. The electron density have been compared to the equivalent width of DIBs and the CH/CH<sup>+</sup> lines. The equivalent width of the CH<sup>+</sup> line drops with rising  $n_e$ , but no changes of the DIBs equivalent widths are observed.

## 2. Column densities and equivalent widths

The aim of this paper is to check the dependences between the electron density and the carriers of DIBs. In order to determine the electron density we had to measure the column densities of two elements in two adjacent ionisation stages. Our target stars were stars fulfilling the following criteria:

- reddened stars of spectral type O or B
- high resolution Hubble Space Telescope (HST) spectra for at least MgI, MgII lines are available (both, GHRS and STIS spectra were used)
- hydrogen column densities are available
- equivalent widths of the chosen DIBs are available

Column densities of Mg I, Mg II, Si I, Si II, C II, C II\* were calculated from high resolution HST spectra. The spectra from the ultraviolet spectral range were downloaded from the HST Data Archive. The GHRS spectra taken in the FP-SPLIT mode were processed with IRAF tasks *poffsets* and *specalign* to achieve the final spectrum. The column densities were derived using the profile fitting technique. The absorption lines were fitted by Voigt profiles. The transitions for which the natural damping constant ( $\Gamma$ ) is not known (Mg II 1240 Å doublet, Mg I 1828 Å) were fitted with a Gauss function. The cloud velocities (v), Doppler broadening parameters (b) and column densities (N) for multiple absorption components were simultaneously fitted to the observed spectrum. Both lines of magnesium doublet (at 1200 Å) were also fitted simultaneously - v, b and N were common for both lines in the doublet. The wavelengths, oscillator strengths (f) and natural damping constants ( $\Gamma$ ) were adopted from Morton (2003).

A convolution with a point spread function (PSF) was also performed. The PSF for the GHRS consists of two Gaussian components. The "core" Gaussian has a FWHM=1.05 diodes, while the "halo" component has FWHM=5.0 diodes (Spitzer & Fitzpatrick (1993)). The relative contribution of the "core" and "halo" components into the PSF is wavelength dependent and was interpolated from the table given by Cardelli *et al.* (1990). The Gaussian PSF for the STIS spectrograph

depends on wavelength, slit and the mode of observations. The tables with FWHM for the combination of mode and slit can be found in "STIS Instrument Handbook" (Kim Quijano (2003)). The FWHM of the Gaussian PSF was wavelength-interpolated from these tables.

The hydrogen (HI) column densities were adopted from Diplas & Savage (1994). Molecular hydrogen ( $H_2$ ) column densities come from Rachford *et al.* (2002) and Savage *et al.* (1977). The equivalent widths of DIBs were kindly supported by Jacek Krełowski.

### 3. Electron density

The electron density ( $n_e$  in  $cm^{-3}$ ) was calculated from the equations of ionisation equilibrium for two elements. The first element was Mg, because it is easily observed in two ionisation stages. The Mg II column density was determined from the 1240 Å doublet, the Mg I column density was determined from the 2026 Å, 2852 Å or 1827 Å line.

The step rise of dielectron recombination coefficient for Mg II with temperature causes the decrease of electron density, inferred from MgI/MgII, with temperature (Fig. 1). Such behaviour enables calculation of electron density, because the curve  $n_e(T_e)$  from MgI/MgII intersects with a curve  $n_e(T_e)$  from another element. The equation of ionisation equilibrium for Mg is the following:

$$\frac{n_e N(Mg\,II)}{N(Mg\,I)} = \frac{\Gamma(Mg_{12}) + n_e C(Mg_{12})}{\alpha_{rad}(Mg_{21}) + \alpha_{die}(Mg_{21})} \quad (1)$$

Where  $N(Mg\,II)$  and  $N(Mg\,I)$  [ $cm^{-2}$ ] are the column densities of ionised and neutral Mg;  $\alpha_{rad}(Mg_{21})$  [ $cm^3/s$ ] is the radiative recombination coefficient;  $\alpha_{die}(Mg_{21})$  [ $cm^3/s$ ] is the dielectronic recombination rate;  $\Gamma(Mg_{12})$  [ $1/s$ ] is the ionisation rate of MgI by UV photons;  $C(Mg_{12})$  [ $cm^3/s$ ] is the collisional ionisation rate.

Because the coefficients  $\alpha_{rad}$ ,  $\alpha_{die}$  and  $C$  depend from electron temperature ( $T_e$ ) we need an analogous equation for a second element to obtain  $n_e$  and  $T_e$  simultaneously. For stars: HD 24534, HD 203374, HD 206267, HD 209339, HD 210839, the second element was Si. The column density of SiI was calculated from the 1845 Å line, and column density of Si II from the 1808 Å one. From the intersection of the  $n_e(T)$  curves from Mg and Si (Fig. 1) we have obtained the electron density.

The  $\Gamma$  coefficients for Mg and Si were adopted from the WJ2 model (de Boer *et al.* (1973)). The recombination coefficients ( $\alpha_{rad}$  and  $\alpha_{die}$ ) and the collisional ionisation rate coefficient ( $C$ ) were adopted from Shull & van Steenberg (1982).

For the stars HD 202904 and HD 160578 the ionisation equilibrium was calculated from MgI/MgII and CII/CII\*. The column density of carbon was calculated from the C II 1335 Å and C II\* 1336 Å lines, using the profile fitting technique (see Gnaciński (2000) for details). The equilibrium between the collisional excitation and radiative de-excitation of ionised carbon is described by the equation (Wood & Linsky (1997)):

$$\frac{N(C\,II^*)}{N(C\,II)} = \frac{n_e C(C_{12})}{\alpha_{rad}(C_{21})} \quad (2)$$

The radiative de-excitation  $\alpha_{rad}(C_{21})$  was adopted from Nussbaumer & Storey (1981). The collision rate coefficient  $C(C_{12})$  was adopted from Wood & Linsky (1997) and Hayes & Nussbauer (1984).

We have also tried to use Ca as the second element for obtaining  $n_e$ . Unfortunately, the CaI/CaII ionisation equilibrium curve (eq. 1) for the stars HD 74455 and HD 149757 does not intersect the ionisation equilibrium curve for Mg I/II. The problem can be caused by the change of  $n(CaII)/n(CaI)$  between the edge and the centre of the cloud. Lepp *et al.* (1988) have found in their numerical simulations, that  $n(CaII)/n(CaI)$  decreases from 4800 at the edge to 160 at the centre of the  $\zeta$  Persei cloud.

#### 4. Results

For a lot of stars Mg is the only element with observations of absorption lines of two stages of ionisation. From the column densities of neutral and ionised Mg we can only calculate the maximal possible electron density  $n_e^{MAX}$ . It is simply the maximum of the  $n_e(T_e)$  curve. Fortunately this maximum ( $n_e^{MAX}$ ) is very well correlated with the electron density  $n_e$  (Fig. 2). The correlation coefficient  $R=0.89$ , and the linear correlation is following:  $n_e^{MAX} = 2.84 \cdot n_e$ . This relation probably reflects the fact, that most of the clouds for which we can calculate  $n_e$  have the electron temperature  $T_e \sim 7500K$ . For stars HD 24912, HD 74455, HD 91316, HD 141637, HD 147165, HD 147933, HD 149757 the electron density was calculated using the  $n_e^{MAX}$  value and this formula. All derived electron densities are presented in Table 3.

Figure 3 presents the relation between the electron density and equivalent widths of the CH and CH+ molecule normalised to the total hydrogen column density. The CH abundance does not change between clouds with various electron density. In opposition to CH, the CH+ abundance is lower for clouds with large electron densities (more recombinations). Such behaviour is also illustrated on Fig. 4, where the theoretical relation between the column densities of Mg I and Mg II are presented versus the electron density.

Figures 5, 6 and 7 presents equivalent widths of DIBs normalised to the total hydrogen column density ( $N(H_{tot})=N(HI)+2N(H_2)$ ) plotted versus electron density ( $n_e$  in  $\text{cm}^{-3}$ ). One could expect a drop of DIBs equivalent width with  $n_e$  as seen on Figure 3 for CH+. Unfortunately, none of the DIBs bands show a relationship with varying electron density. There are two possible explanations for the lack of relationship between DIBs and  $n_e$ . First explanation, that the carriers of the analysed DIBs may be observed only in one ionisation stage. At Figure 4 we can see such behaviour for Mg II. In a wide range of observed electron densities ( $n_e=0.008-2.4 \text{ cm}^{-3}$ ) the column density of Mg II does not change by a considerable amount. Such behaviour is also seen for CH on Figure 3. The second explanation is that DIBs arise in parts of interstellar clouds where we observe only one stage of ionisation of Mg and other elements. The DIBs can arise in dense cores of interstellar clouds, where ionised atoms are hardly observed. DIBs may also arise

at outer (ionised) parts of the interstellar clouds, where neutral elements are absent. For both cases we can not calculate the electron density.

## 5. Conclusions

The results can be recapitulated as follows:

1. The electron density in the interstellar clouds was determined for 13 lines of sight.
2. Linear correlation between the electron density and maximum possible value of electron density from MgI/MgII was found.
3. The normalised equivalent width of the CH+ line drops with rising electron density as expected from the ionisation equilibrium.
4. The normalised equivalent widths of the 5780Å, 5797Å, 6614Å, 5850Å, 5844Å, 6203Å, 6270Å, 6284Å, 6376Å, 6379Å, 6660Å, 6196Å DIBs do not change with varying electron density.

*Acknowledgements.* We are very grateful to Jacek Krełowski for the equivalent widths of the DIBs and the CH/CH+ lines. This publication is based on observations made with the NASA/ESA Hubble Space Telescope, obtained from the data archive at the Space Telescope Science Institute. STScI is operated by the Association of Universities for Research in Astronomy, Inc. under NASA contract NAS 5-26555.

## References

- de Boer K.S., Koppenaal K. & Pottasch S.R., 1973, A&A, 28, 145
- Bohlin R.C., Savage B.D., Drake J.F., 1978, ApJ, 224, 132
- Cami J., Salama F., Jiménez-Vicente J., Galazutdinov G.A., Krełowski J., 2004, ApJ, 611, L116
- Cardelli, J.A., Ebbets, D.C., Savage, B.D., 1990, ApJ, 365, 789
- Chlewicki G., van der Zwet G.P., nav Ijzendoorn L.J., Greenberg J.M., Alvarez P.P., 1986, ApJ, 305, 455
- Cox N.L.J., Spaans M., 2006, A&A, 451, 973
- Diplas A., Savage B.D., 1994, ApJS, 93, 211
- Frisch P.C., York D.G., Fowler J.R., 1987, ApJ, 320, 842
- Galazutdinov G.A., Moutou C., Musaev F.A., Krełowski J., 2002, A&A, 384, 215
- Galazutdinov G.A., Musaev F.A., Krełowski J., Walker G.A.H., 2000, PASP, 112, 648
- Gnaciński P., 2000, Acta Astron., 50, 133
- Hayes M.A. & Nussbauer H., 1984, A&A, 134, 193
- Herbig G.H., 1995, ARA&A, 33, 19
- Jenkins E.B., Savage B.D., Spitzer L., 1986, ApJ, 301, 355
- Kim Quijano, J. *et al.*, 2003, "STIS Instrument Handbook" (Baltimore: STScI), available at:  
<http://www.stsci.edu/hst/stis/documents>
- Krełowski J., et al., 1999, A&A, 347, 235
- Krełowski J., 1989, Astron. Nachr., 310, 255
- Lepp S., Dalgarno A., van Dishoeck E.F., Black J.H., 1988, ApJ, 329, 418
- Lacour S., André, M.K., Sonnentrucker, P., *et al.*, 2005, A&A, 430, 967

Star	MgI	MgII	SiI	SiII	CII & CII*
HD 24534	z2do0209t o66p07010 o66p03010	z2do0107t	o66p03010 o66p03020	z2do0208t o66p03010 o66p03020	
HD 24912	z0gy011ft z0de010vt	z0gy010kt			
HD 74455	z37j030kt z37j0305t	z37j030jt			
HD 91316	z0zi030d,e,f,g	z2zx0108t			
HD 141637	z0vo030d,e,f,g	z2zx5208t			
HD 147165	z13v020a,b,c z13v020d,e,f	z34r0407t			
HD 149757	z0rz020rt z0ld021ct	z2vx0109a,b			
HD 160578	z2xt020dt z2xt020jt	z2xt010at			z2xt010et
HD 202904	z2xu0308t	z2xt0308t			z2xt030et
HD 203374	o5lh08040,50,60	o5lh08010,20,30 o6lz90010	o5lh08040,50,60	o5lh08040,50,60	
HD 206267	o5lh09030,40	o5lh09010,20	o5lh09030,40	o5lh09030,40	
HD 209339	o5lh0b030,40	o5lh0b010,20	o5lh0b030,40	o5lh0b030,40	
HD 210839	o54304020	o54304010	o54304020	o54304020	

**Table 1.** HST spectra used to derive column densities of the Mg, Si and C elements.

Morton, D.C., 2003, ApJSS, 149, 205

Moutou C., Krełowski J., d'Hendecourt L., Jamrożczak J., 1999, A&A, 351, 680

Nussbaumer H., Storey P.J., 1981, A&A, 96, 91

Omert A., 1986, A&A, 164, 159

Rachford B.L., et al., 2002, ApJ, 577, 221

Savage B.D., Bohlin R.C., Drake J.F., Budich W., 1977, ApJ, 216, 291

Shull J.M. & van Steenberg M., 1982, ApJS, 48, 95

Sonnentrucker P., Cami J., Ehrenfreud P., Foing B.H., 1997, A&A, 327, 1215

Spitzer, L.Jr., Fitzpatrick, E.L., 1993, ApJ, 409, 299

Weselak T., Fulara J., Schmidt M.R., Krełowski J., 2001, A&A, 377, 677

Wood B.E., Linsky J.L., 1997, ApJ, 474, L39

van der Zwet G.P., Allamandola L.J., 1985, A&A, 146, 76

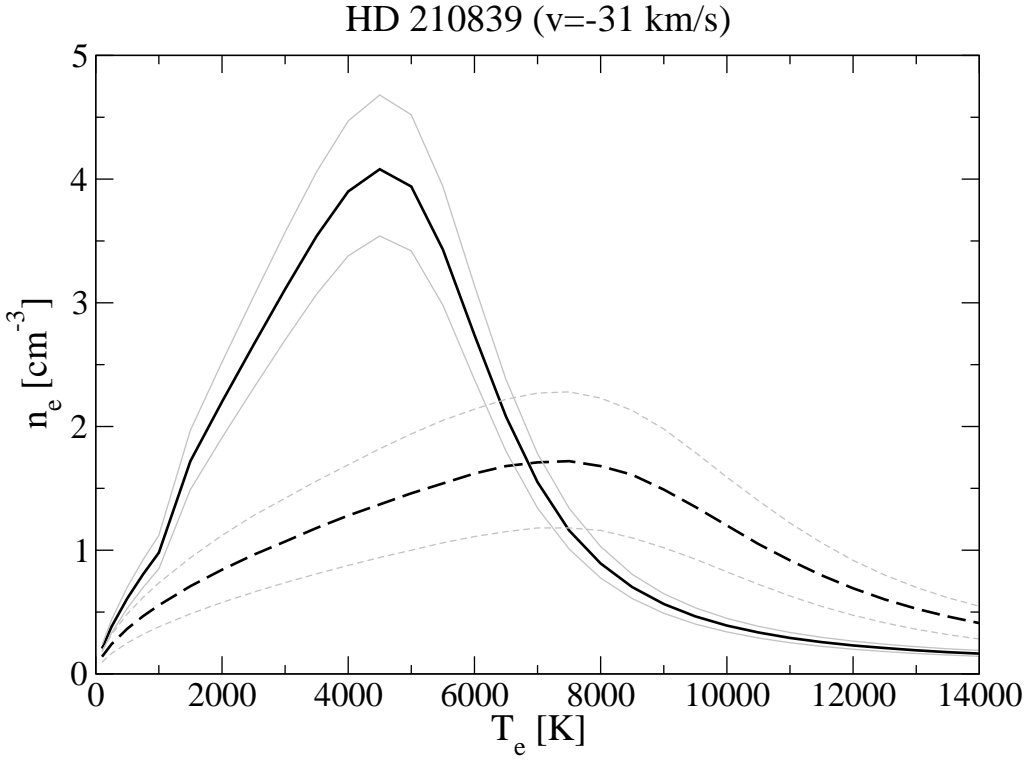


**Fig. 1.** The  $n_e(T_e)$  curves from MgI/MgII (solid line) and SiI/SiII (dashed line) for the  $v =$

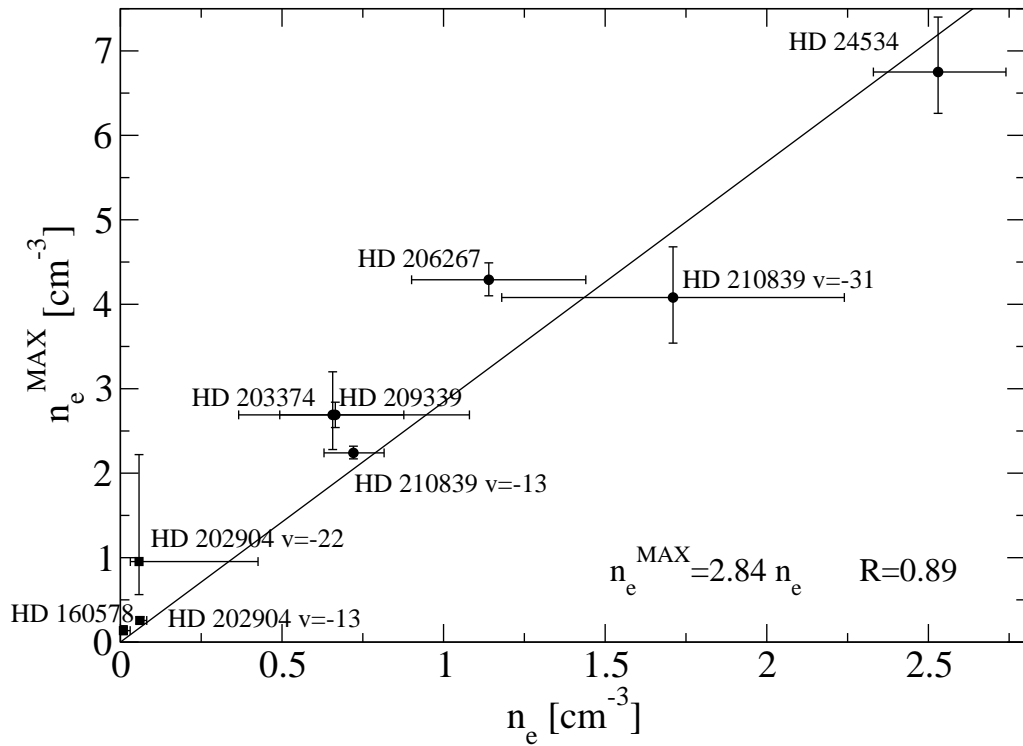


**Fig. 2.** The linear correlation between maximum  $n_e$  from the  $N(MgII)/N(MgI)$  and the exact  $n_e$  value.

	$\Gamma$ [1/s]	$C(T)$ [ $cm^3/s$ ]	$\alpha_{rad}(T)$ [ $cm^3/s$ ]	$\alpha_{die}(T)$ [ $cm^3/s$ ]
Mg I/II	$8.1 \cdot 10^{-11}$	$8.9 \cdot 10^{-11} \sqrt{T} (1 + 0.1 \cdot T/88700)^{-1} \cdot exp(-88700/T)$	$1.4 \cdot 10^{-13} \cdot (T/10000)^{-0.855}$	$4.49 \cdot 10^{-4} T^{-3/2} exp(-50100/T) \cdot (1 + 0.021 \cdot exp(-28100/T))$
Si I/II	$3.8 \cdot 10^{-9}$	$3.92 \cdot 10^{-10} \sqrt{T} (1 + 0.1 \cdot T/94600)^{-1} \cdot exp(-94600/T)$	$5.9 \cdot 10^{-13} \cdot (T/10000)^{-0.601}$	$1.1 \cdot 10^{-3} T^{-3/2} exp(-77000/T)$
Ca I/II	$3.8 \cdot 10^{-10}$	$2.09 \cdot 10^{-10} \sqrt{T} (1 + 0.1 \cdot T/70900)^{-1} \cdot exp(-70900/T)$	$1.12 \cdot 10^{-13} \cdot (T/10000)^{-0.9}$	$3.28 \cdot 10^{-4} T^{-3/2} exp(-34600/T) \cdot (1 + 0.0907 \cdot exp(-16400/T))$
C II/II*	—	$8.63 \cdot 10^{-6} (2 \sqrt{T})^{-1} \Omega_{12}(T) \cdot exp(-\frac{1.31 \cdot 10^{-14} erg}{kT})$	$2.29 \cdot 10^{-6}$	—

**Table 2.** Parameters used in the ionisation equilibrium equation. The ionisation rate  $\Gamma$  was adopted from the WJ2 model of de Boer *et al.* (1973). The recombinations rates  $\alpha_{rad}$  and  $\alpha_{die}$  as well as the collisional ionisation rate  $C$  for Mg, Si and Ca was adopted from Shull & van Steenberg (1982). The  $\alpha_{rad}(CII)$  comes from Nussbaumer & Storey (1981). The collision strength  $\Omega_{12}(T)$  was fitted by an 8-order polynomial to the data given by

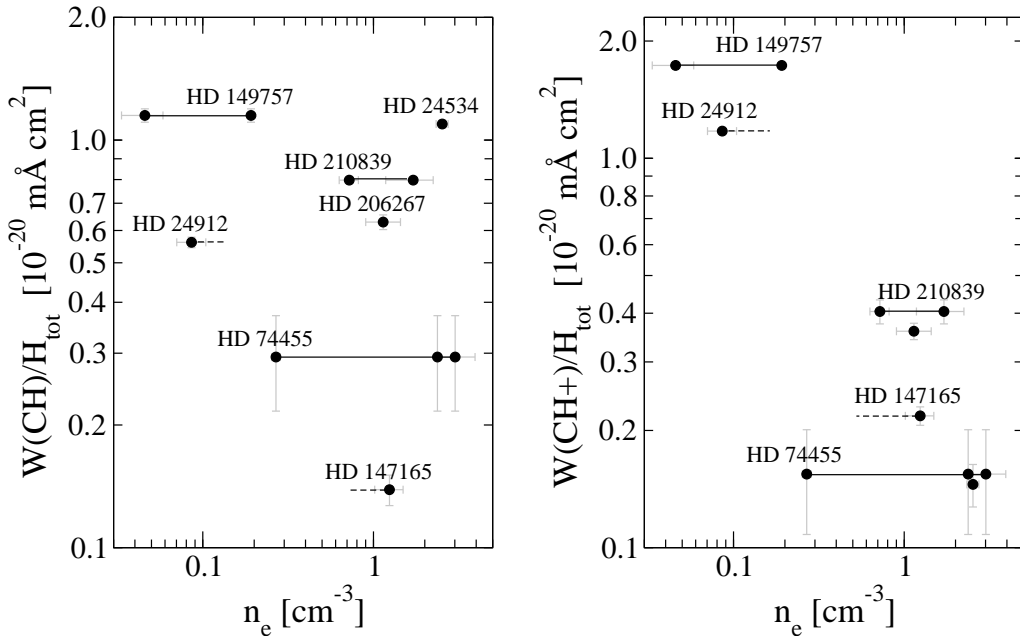


**Fig. 3.** The equivalent widths of the CH and CH+ spectral lines normalised to the total hydrogen column density are plotted versus electron density ( $n_e$ ). The solid lines connect points from different clouds in the direction of one star. The dashed lines indicates second cloud with undeterminable electron density.

Star	v [km/s]	$n_e$ [cm $^{-3}$ ]	$n_e^{MAX}$ [cm $^{-3}$ ]	HI ref [logN(HI)]	H $_2$ ref [logN(H $_2$ )]	CH $^+$ [mÅ]	CH [mÅ]
HD 24534	18	$2.5^{+0.2}_{-0.2}$	$6.7^{+0.6}_{-0.6}$	20.73	3	$20.92 \pm 0.4$	$24.1 \pm 0.5$
HD 160578	-27	$0.009^{+0.02}_{-0.004}$	$0.14^{+0.06}_{-0.05}$	20.19	3		
HD 202904	-22	$0.06^{+0.38}_{-0.03}$	$0.9^{+1.3}_{-0.4}$	20.68	4	$19.15 \pm 0.4$	
HD 202904	-13	$0.06^{+0.02}_{-0.01}$	$0.26^{+0.04}_{-0.04}$				
HD 203374	-18	$0.66^{+0.22}_{-0.16}$	$2.7^{+0.5}_{-0.4}$				
HD 206267	-13	$1.1^{+0.3}_{-0.2}$	$4.3^{+0.2}_{-0.2}$	21.30	5	$20.86 \pm 0.8$	$21.7 \pm 0.9$
HD 209339	-15	$0.7^{+0.4}_{-0.3}$	$2.7^{+0.2}_{-0.2}$				
HD 210839	-31	$1.7^{+0.5}_{-0.5}$	$4.1^{+0.6}_{-0.5}$	21.15	3	$20.84 \pm 0.8$	$22.3 \pm 0.4$
HD 210839	-13	$0.72^{+0.1}_{-0.09}$	$2.24^{+0.08}_{-0.07}$				
Directions with the electron density calculated with the formula $n_e = n_e^{MAX} / 2.84$ from the Mg column densities.							
HD 24912	14	$0.09^{+0.02}_{-0.02}$	$0.24^{+0.05}_{-0.04}$	21.05	3	$20.53 \pm 0.19$	$10.1 \pm 0.3$
HD 74455	25	$0.27^{+0.02}_{-0.02}$	$0.76^{+0.05}_{-0.04}$	20.73	3	$19.74 \pm 0.3$	$1.9 \pm 0.5$
HD 74455	5	$3.0^{+0.9}_{-0.6}$	$8.6^{+2.6}_{-1.7}$				
HD 74455	-160	$2.4^{+0.09}_{-0.08}$	$6.7^{+0.3}_{-0.2}$				
HD 91316	-8	$0.17^{+0.02}_{-0.02}$	$0.48^{+0.07}_{-0.07}$	20.44	3	$15.61 \pm 0.7$	
HD 91316	17	$0.17^{+0.04}_{-0.04}$	$0.5^{+0.1}_{-0.1}$				
HD 141637	-7	$0.109^{+0.005}_{-0.004}$	$0.31^{+0.01}_{-0.01}$	21.18	3	$19.23 \pm 0.4$	
HD 141637	-12	$0.12^{+0.02}_{-0.02}$	$0.33^{+0.07}_{-0.05}$				
HD 147165	-9	$1.2^{+0.3}_{-0.2}$	$3.5^{+0.7}_{-0.6}$	21.38	3	$19.79 \pm 0.2$	$4.5 \pm 2.9$
HD 149757	-17	$0.192^{+0.005}_{-0.006}$	$0.54^{+0.02}_{-0.02}$	20.69	3	$20.65 \pm 0.2$	$22.4 \pm 18.0$
HD 149757	-29	$0.046^{+0.013}_{-0.012}$	$0.13^{+0.04}_{-0.04}$				

**Table 3.** The electron densities derived for target stars. The equivalent widths of the CH $^+$  and CH lines were adopted from Krełowski *et al.* (1999). References: (1)-Rachford *et al.* (2002) ; (2)-Savage *et al.* (1977) ; (3)-Diplas & Savage (1994) ; (4)-Jenkins *et al.* (1986) ; (5)-Lacour *et al.* (2005) ; (6) - N(H $_2$ ) calculated from the formula : N(H $_2$ ) =  $2.9e19 \cdot W(CH)$ ; (7)-Bohlin *et al.* (1978) ; .

Star	5797	5780	5850	5844	6196	6203	6270	6284	6376	6379	6614	6660
HD 24534	$62.5 \pm 3.1$	$96.2 \pm 9.5$	$27.7 \pm 2.3$		$16.9 \pm 1.9$	$32.2 \pm 4.8$	$33.6 \pm 6.9$	$73.3 \pm 11$	$30.6 \pm 4.6$	$50.6 \pm 3.8$	$65.7 \pm 3.6$	$12.7 \pm 1.7$
HD 202904	$8 \pm 1.5$	$44 \pm 3.5$			$6 \pm 0.5$	$11 \pm 1.3$	$10 \pm 2$	$96 \pm 15$			$19 \pm 2.5$	
HD 206267	$89.8 \pm 1.6$	$222.7 \pm 3.6$	$44.9 \pm 2.8$		$27.3 \pm 0.5$	$44.2 \pm 1.5$	$72.9 \pm 4.1$	$199.2 \pm 4.6$	$25.5 \pm 1.5$	$36.3 \pm 0.9$	$117 \pm 1.1$	$20.3 \pm 0.8$
HD 210839	$71.2 \pm 0.9$	$253.1 \pm 2.7$	$60.9 \pm 2.4$		$30.7 \pm 1.1$	$53.8 \pm 2.5$	$90.2 \pm 3.3$	$482 \pm 26$	$23.9 \pm 2$	$55.9 \pm 1.3$	$147.2 \pm 2.5$	$25.5 \pm 0.9$
HD 24912	$36.1 \pm 0.6$	$200.3 \pm 2.4$	$29.1 \pm 1$	37.1	$20.7 \pm 0.4$	$22.9 \pm 1$	$23 \pm 1.1$	$197 \pm 3.5$	$12 \pm 1.6$	$26 \pm 1.4$	$77.6 \pm 2.5$	$16 \pm 1$
HD 74455	$13 \pm 3$	$31 \pm 5$			$4.5 \pm 1$	$6.5 \pm 1.5$	$12 \pm 3$	$105 \pm 13$		$2.3 \pm 1$	$17.5 \pm 2$	$1.5 \pm 0.5$
HD 91316	$17 \pm 3$	$32 \pm 5$			$4 \pm 1$	$15 \pm 3$	$19 \pm 5$	$50 \pm 8$				
HD 141637	$8.1 \pm 0.8$	$78 \pm 3$			$7.3 \pm 1$	$11 \pm 1.5$	$11 \pm 3$	$220 \pm 14$		$3.5 \pm 1$	$16.5 \pm 2$	
HD 147165	$26.3 \pm 4.9$	$243.3 \pm 3.1$	$9.9 \pm 0.5$		$16.5 \pm 0.5$	$18.9 \pm 0.8$	$14 \pm 1.1$	$142.6 \pm 2.1$	$9.5 \pm 0.5$	$20.1 \pm 0.3$	$60.9 \pm 1.2$	$8.1 \pm 0.5$
HD 147933	$50.8 \pm 2.4$	$208 \pm 12.5$	$28.1 \pm 0.8$	20.3	$16.6 \pm 0.7$	$22.8 \pm 1.3$	$20 \pm 1.3$	$176.4 \pm 2.8$	$11.6 \pm 0.8$	$25.9 \pm 1$	$64.6 \pm 1.7$	$11.8 \pm 0.9$
HD 149757	$30.5 \pm 1.5$	$66.4 \pm 1.9$	$15.7 \pm 1.5$	10.8	$11 \pm 0.5$	$14.5 \pm 0.8$	$13.1 \pm 1$	$68.2 \pm 2$	$3.5 \pm 0.3$	$18.7 \pm 0.5$	$40.5 \pm 2$	$4.2 \pm 0.4$

**Table 4.** Equivalent widths of the diffuse interstellar bands in mÅ (courtesy of Jacek Krełowski).

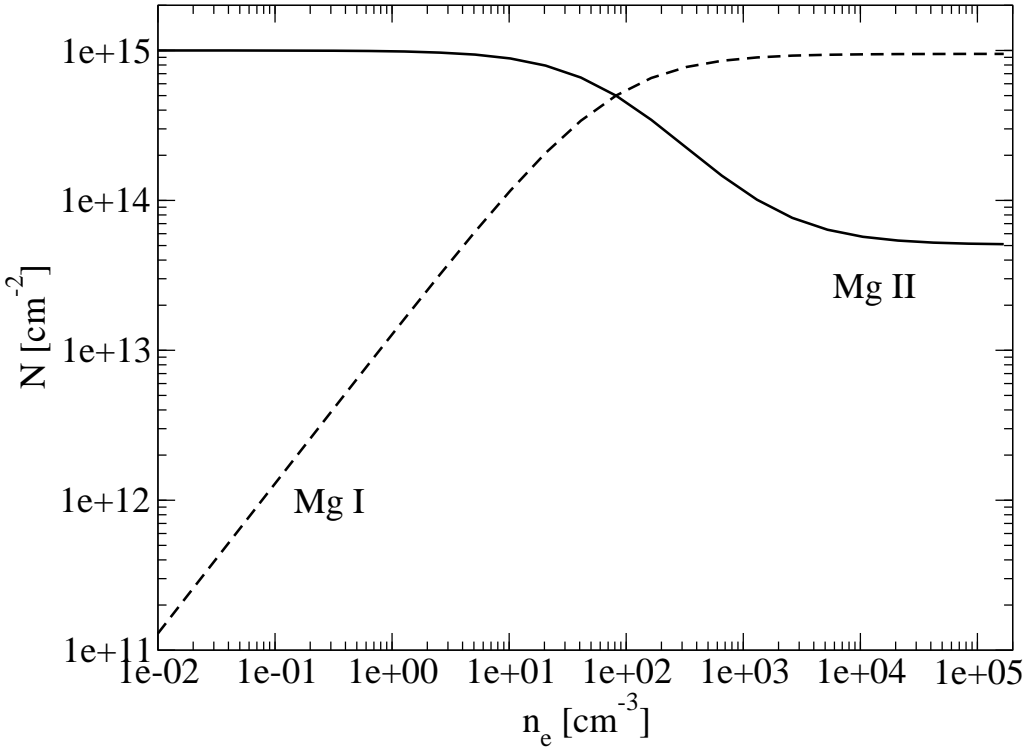


**Fig. 4.** Theoretical relation between the magnesium column density and the electron density  $n_e$ .

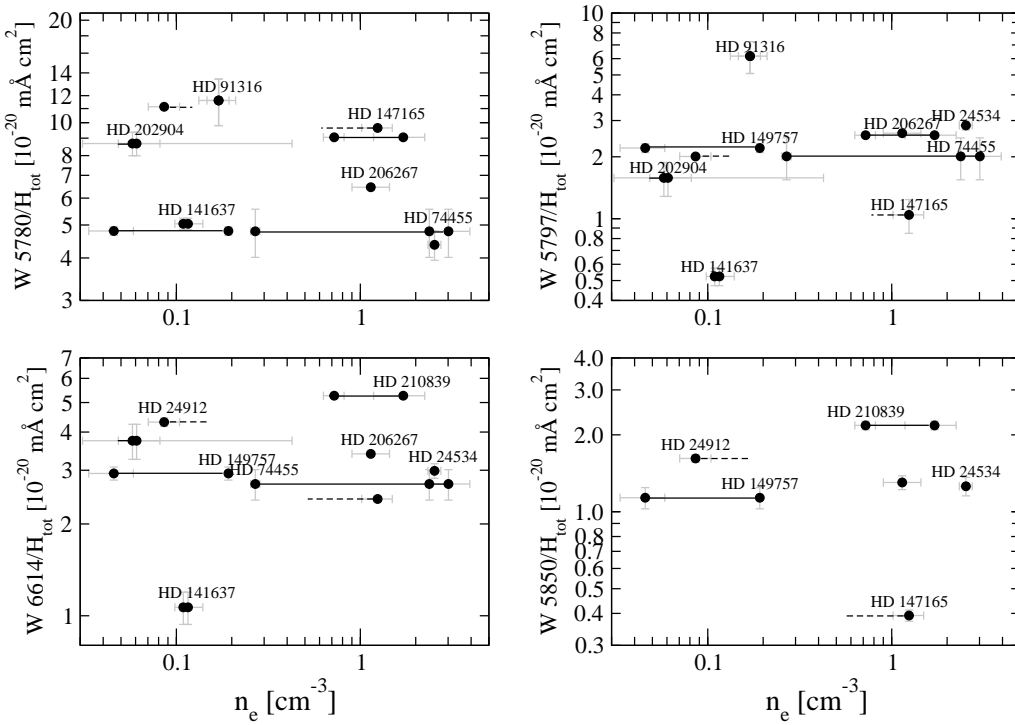


**Fig. 5.** The equivalent widths of DIBs normalised to the total hydrogen column density are plotted versus electron density ( $n_e$ ). The solid lines connect points from different clouds in the direction of one star. The dashed lines indicates second cloud with undeterminable electron density.

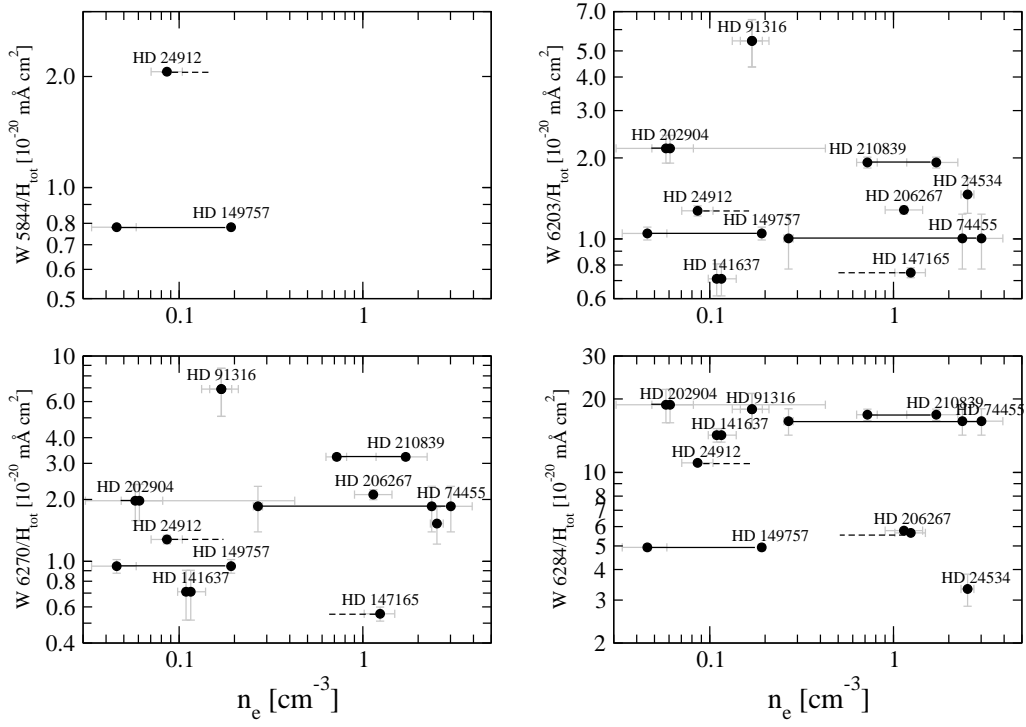


**Fig. 6.** The equivalent widths of DIBs normalised to the total hydrogen column density are plotted versus electron density ( $n_e$ ). The solid lines connect points from different clouds in the direction of one star. The dashed lines indicates second cloud with undeterminable electron density.

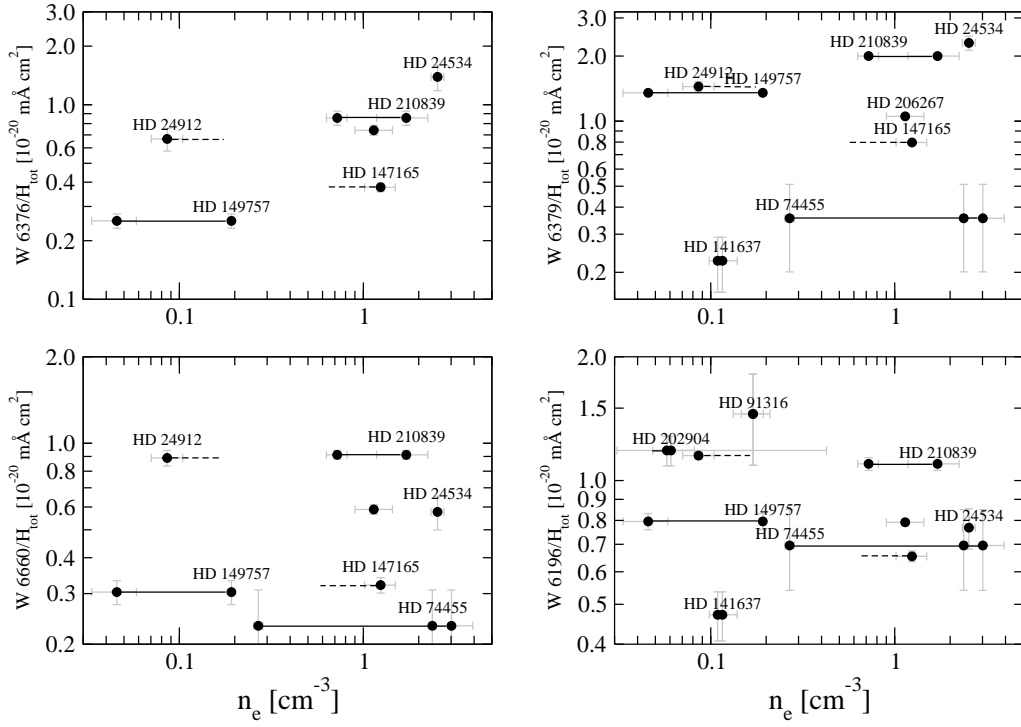


**Fig. 7.** The equivalent widths of DIBs normalised to the total hydrogen column density are plotted versus electron density ( $n_e$ ). The solid lines connect points from different clouds in the direction of one star. The dashed lines indicates second cloud with undeterminable electron density.